Journal of Hazardous Materials 201–202 (2012) 170–177

Contents lists available at SciVerse ScienceDirect

Journal of Hazardous Materials

journal homepage: www.elsevier.com/locate/jhazmat

Self-assembled mesoporous γ-Al_2O_3 spherical nanoparticles and their efficiency for the removal of arsenic from water

Astam K. Patra, Arghya Dutta, Asim Bhaumik*

Department of Materials Science, Indian Association for the Cultivation of Science, Jadavpur, Kolkata 700032, India

ARTICLE INFO

Article history:
Received 1 June 2011
Received in revised form
16 November 2011
Accepted 17 November 2011
Available online 25 November 2011

Keywords:
Mesoporous material
Nanoparticle
Templated synthesis
Adsorption
γ-Al_2O_3

ABSTRACT

We report a highly efficient synthetic strategy for self-assembled mesoporous γ-Al_2O_3 materials using sodium salicylate as template. The mesoporous γ-Al_2O_3 samples synthesized following this strategy have high surface areas (231–497 $m^2\,g^{-1}$), consist of crystalline tiny spherical nanoparticles of dimensions *ca.* 2–10 nm and showed high affinity for the adsorption of arsenic from the contaminated aqueous solutions. Efficient synthesis strategy, exceptionally high surface area and high adsorption efficiency of these mesoporous γ-Al_2O_3 materials for the dissolved arsenic from the contaminated aqueous solutions (in the form of oxyanions of arsenic) could find potential utility in the purification of polluted water.

© 2011 Elsevier B.V. All rights reserved.

1. Introduction

Unique surface properties of metal oxide nanoparticles of definite shape and size have motivated the researchers to explore new synthesis strategies for the nanostructured materials under controlled synthesis conditions [1–3]. In the solution based sol–gel synthetic pathway usually a capping agent is used to control the crystallization of the nuclei to a particular shape and size, and thus to achieve desired material properties [4–6]. Although, the capping agent could direct the synthesis of very tiny nanocrystals, its removal from the nanocomposites often causes agglomeration of the tiny particles, resulting in a loss of surface area. Thus a convenient synthesis route for designing a nanomaterial, having large surface area is highly desirable. Among the metal oxides studied in this context, Al_2O_3 is one of the most intensively investigated due to its wide-scale potentials in catalysis [7–11], optics [12], electronics [13], adsorption [14] and biomedical applications [15].

Due to the electron deficiency at the surface, nanostructured Al_2O_3 has strong affinity for the target anions and thus it can be used as absorbents for the removal of hazardous/toxic metal oxyanions. Heavy metal ions and specially arsenic is a serious environmental problem worldwide and its long term exposure in drinking water can cause cancer in skin, lungs, kidney and cardiovascular diseases [16,17]. Contamination of arsenic via natural reaction, biological activity, geochemical reaction and volcanic emission causing contamination level of arsenic much larger than that recommended by World Health Organization (WHO) in drinking water (0.01 mg/L) [18]. Arsenic is generally present in the ground water as arsenite ($AsO_3{}^{3-}$/$AsO_2{}^{-}$) or arsenate ($AsO_4{}^{3-}$) oxyanions [19]. Thus electron deficiency or Lewis acidic property at the surface of Al_2O_3 nanoparticles could be utilized for the adsorption of these oxyanions of arsenic through electrostatic interactions [20–23].

However, one of the major problems associated with Al_2O_3 based nanostructured material in the adsorption application is its low surface area. In order to enhance the adsorption efficiency surface area and thus nanoscale porosity at the surface of Al_2O_3 material have to be greatly enhanced [24]. Thus mesoporous alumina, which is less expensive, easier and safer to handle can be a potential adsorbent for the removal of dissolved arsenic from polluted ground water. Nonionic diblock or triblock poly(ethylene oxide) surfactants [25], triblock copolymer/ethanol [26], etc. are used as the structure-directing porogens or templates for introducing mesoporosity in alumina. However, designing uniform tiny nanocrystals of alumina material together with its high surface area is still a challenge today. Very recently we have designed the synthesis of self-assembled TiO_2 spherical nanoparticles having exceptionally high surface area by using sodium salicylate as template [27]. In this paper, we present a method to synthesize very tiny self-assembled mesoporous γ-Al_2O_3 spherical nanoparticles by using sodium salicylate as template. Oxyanions of arsenic could be trapped at the Lewis acidic surface of mesoporous γ-Al_2O_3 through electrostatic interactions and thus the self assembled

* Corresponding author. Tel.: +91 33 2473 4971.
E-mail address: msab@iacs.res.in (A. Bhaumik).

0304-3894/$ – see front matter © 2011 Elsevier B.V. All rights reserved.
doi:10.1016/j.jhazmat.2011.11.056

mesoporous γ-Al_2O_3 nanomaterial could be utilized as adsorbent for the removal of arsenic from contaminated water.

2. Experimental

Self-assembled γ-Al_2O_3 nanomaterials were synthesized by employing the following procedure. In this typical synthesis, 2.0 g ammonium chloride (37.4 mmol, E-Merck, 98.9% GR) was added to a 20 mL aqueous solution consisting of 1.6 g sodium salicylate (SS: 10 mmol, E-Merck, 99.5%). The solution was stirred for 15 min. Then 4 mL ammonia solution (25% aqueous) was added and the mixture was stirred again for 30 min. Then 1.33 g anhydrous $AlCl_3$ (10 mmol, E-Merck) was dissolved in 5.0 g distilled water and this solution was slowly added to the above solution. The pH of the solution was adjusted to *ca.* pH = 10 by addition of ammonia solution and the resulting mixture were stirred for 3 h. Then the mixture was transferred into a Teflon-lined stainless steel autoclave and hydrothermally treated at 393 K for 24 h. The light yellow solid was collected through filtration, washed with water, dried at room temperature under vacuum and the material has been designated as MA-1. Further, the syntheses were also carried out at two other temperatures, at 353 and 273 K and, corresponding mesoporous alumina samples are designated as MA-2 and MA-3, respectively. All the as-synthesized samples were calcined at 773 K for 6 h to remove the template molecules and thus to generate mesoporosity. Corresponding calcined materials were designated as MA-1C, -2C and -3C, and these samples were used in the adsorption studies.

Adsorption experiments were carried out over mesoporous γ-Al_2O_3 materials using aqueous sodium arsenite solutions of known strengths *ca.* 10–400 ppb. Apart from these stock solutions we have collected three different ground water samples from the deep tube-wells located in different parts of West Bengal, India and used our mesoporous alumina samples as adsorbent for the removal of arsenic from these solutions. In all cases the adsorption experiments are conducted for 6 h at room temperature (298 K) under vigorous stirring. For all these experiments 0.1 g sample (adsorbent, mesoporous γ-Al_2O_3 material) was used. After removing the adsorbent through filtration, the initial and the final concentration of arsenic in these solutions were measured through AAS analysis. Upon subtracting the final arsenic content from initial one, the adsorption amounts for different samples has been calculated (Table 1). To understand the stability and efficiency of our self-assembled mesoporous γ-Al_2O_3 materials for repeated adsorption studies, we have collected the adsorbent after every experiment (using MA-1C as representative) and washed with KCl solution to remove the adsorbed arsenic (in the form of arsenite oxyanion) from the materials, dried and characterized by powder XRD.

The adsorption kinetics for arsenic(III) and arsenic(V) were studied over the mesoporous alumina sample MA-1C. In these experiments 0.1 adsorbent was dispersed in 100 mL of *ca.* 100 ppb arsenite solution and stirred vigorously for 1 h. After the 1 h, the solution was filtered and the concentration of the solution was measured through AAS analysis. We have performed the similar adsorption experiments by taking out the adsorbents after 2, 3, 4, 5 and 6 h from another five set of experiments. The adsorption kinetics of arsenate was also studied similarly over MA-1C following the same procedure. The arsenate solution was prepared from the arsenite solution via oxidation in the presence of H_2O_2 as the oxidizing agent. For oxidation of arsenite solution, 1 g H_2O_2 (Merck, 35%) was added in 250 mL arsenite solution and stirred for 2 h to get the corresponding arsenate solution. For the pH dependent study, we have prepared 250 mL *ca.* 10^4 ppb arsenite solution by dissolving 4.33 mg $NaAsO_2$ in 250 mL double distilled water. Now for preparation of 100 ppb solution having pH = 4, 1.0 mL of this solution was diluted with 99 mL buffer solution (pH = 4) and the resulting solution was used for adsorption measurement. Similarly the adsorption experiments were also performed at pH = 5–7 and 9, using the respective buffer solutions.

Powder X-ray diffraction patterns of the samples were recorded on a Bruker D-8 Advance diffractometer operated at 40 kV voltage and 40 mA current using Cu K_α (λ = 0.15406 nm) radiation. TEM images were recorded in a JEOL 2010 TEM operated at 200 kV. A JEOL JEM 6700F field emission scanning electron microscope (FE SEM) was used for the determination of particle morphology. Nitrogen sorption isotherms were obtained using a Belsorp HP surface area analyzer at 77 K. Prior to the measurement, the samples were degassed at 393 K for 12 h. Thermogravimetric (TG) and differential thermal analyses (DTA) of the samples were carried out in a TA Instruments thermal analyzer TA-SDT Q-600. Arsenic content in different stock solutions and ground water samples were estimated by using a Shimadzu AA-6300 atomic absorption spectrometer (AAS) fitted with a double beam monochromator. UV–visible

Table 1
Adsorption of arsenic by mesoporous γ-Al_2O_3 materials.

Sample	Anion	Anion content in solution (ppb)		Anion removal efficiency (%)	Distribution coefficient (K_d)[a] (mL/g)
		Before	After		
MA-1C	AsO_2^-	400	105.2	73.7	2.83×10^3
		200	74.3	63.9	1.83×10^3
		100	25.0	75.0	3.00×10^3
		10	2.1	79.0	4.00×10^3
	Sample 1[b]	257	39.2	84.7	5.50×10^3
	Sample 2[c]	50.45	6.89	86.3	6.32×10^3
	Sample 3[d]	27.28	4.58	83.2	4.95×10^3
MA-2C	AsO_2^-	400	126.6	68.4	2.25×10^3
		200	85.1	57.5	1.43×10^3
		100	33.2	66.8	2.00×10^3
		10	2.5	75.0	3.00×10^3
	Sample 1[b]	257	48.4	79.7	4.30×10^3
	Sample 2[c]	50.45	9.35	81.4	4.31×10^3
	Sample 3[d]	27.28	5.85	78.2	3.66×10^3
Al_2O_3[e]	AsO_2^-	100	47.32	52.6	1.11×10^3

[a] Distribution coefficient (K_d) between solid and aqueous phase = number of cations adsorbed per g of the solid/number of cations present per mL solution after exchange. $K_d = C_{solid}/C_{water}$ (mol g^{-1}/mol mL^{-1}) = C_{solid}/C_{water} (mL/g).
[b] Ground water sample collected from the deep tube-wells located in South 24 Parganas.
[c] Ground water sample collected from the deep tube-wells located in Jadavpur.
[d] Ground water sample collected from the deep tube-wells located in Hooghly, West Bengal, India.
[e] Commercial Al_2O_3.

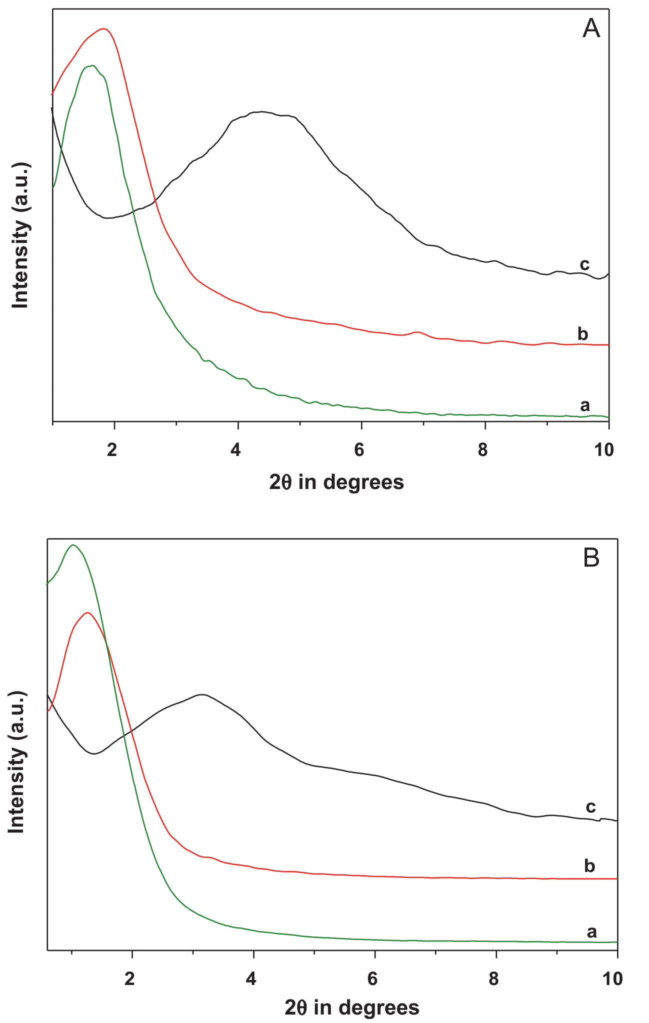

Fig. 1. (A) Small angle XRD patterns of as-synthesized MA-1 (a), MA-2 (b) and MA-3 (c). (B) Small angle XRD patterns of calcined MA-1C (a), MA-2C (b) and MA-3C (c).

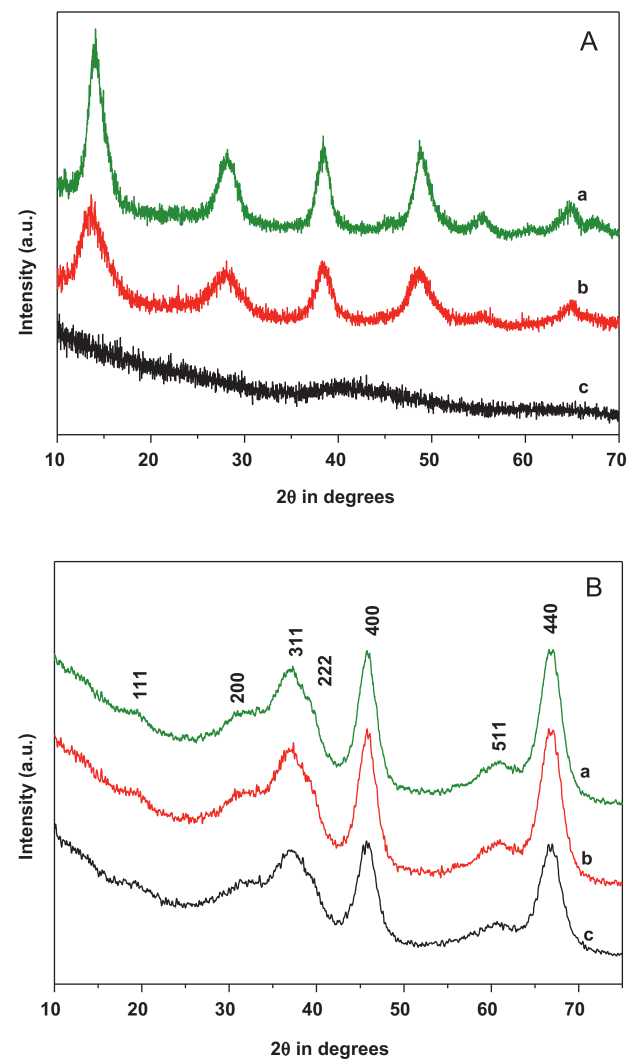

Fig. 2. (A) Wide angle XRD patterns of as-synthesized MA-1 (a), MA-2 (b) and MA-3 (c). (B) Wide angle XRD patterns of calcined MA-1C (a), MA-2C (b) and MA-3C (c).

diffuse reflectance spectra were recorded on a Shimadzu UV 2401PC with an integrating sphere attachment. $BaSO_4$ was used as background standard.

3. Results and discussion

3.1. Characterization of γ-Al_2O_3 nanomaterials

Small angle powder XRD patterns of the as-synthesized and calcined mesoporous Al_2O_3 samples are shown in Fig. 1A and B, respectively. One broad peak signifying the average particle-center-to-particle-center correlation length is observed for all the samples. However, very interestingly increasing the synthesis temperature from 273 to 393 K distance between particle-center-to-particle-center drastically increased from 2.8 nm to 8.7 nm as seen from the respective powder diffraction patterns (Fig. 1B). The increase of this interparticle distance is related to the increase in particle size for the high temperature synthesis (see TEM analysis below). At higher temperature the condensation and growth of the particles is favored and this result agrees well with our self-assembled mesoporous TiO_2 nanospheres templated by sodium salicylate template [27]. The wide angle XRD pattern of the Al_2O_3 nanoparticles (Fig. 2B) suggested that the γ-Al_2O_3 nanoparticles are highly crystalline. Crystalline planes corresponding to the peaks for γ-Al_2O_3 have been indexed. All calcined samples show major peaks at 2θ values of 19.45°, 31.93°, 37.60°, 39.49°, 45.86°, 60.89° and 67.03°, which correspond to γ-Al_2O_3 (1 1 1), (2 0 0), (3 1 1), (2 2 2), (4 0 0), (5 1 1) and (4 4 0) crystal planes, respectively (JCPDS PDF No. 10-0425) [28]. Thus these powder XRD results revealed that we have synthesized highly stable and crystalline γ-Al_2O_3 spherical nanomaterials while using sodium salicylate as a template.

On the other hand, while removing the template molecules through calcination this *d*-spacing increases in contrast to conventional surfactant-templated mesoporous materials, where contraction of the pore wall (and *d*-spacings) occurred [29–32]. Here the positively charged γ-Al_2O_3 spherical nanoparticles are held together by the salicylate moieties at its periphery (Fig. 3). Under the synthesis conditions alumina nanoparticles are positively charged and could interact with the negatively charged carboxylate groups of sodium salicylate molecules through electrostatic interaction as shown in Fig. 3. Presence of the ortho phenolic –OH group in the salicylate molecule under synthesis condition in turn helps to form supramolecular assembly among the ligated salicylate moieties via hydrogen bonding and hydrophobic interactions [27]. This supramolecular assembly of the salicylate molecules helps to form the cage like structure inside the γ-Al_2O_3 nanocrystals. Upon calcination these salicylate molecules get removed and high temperature causes further condensation, and

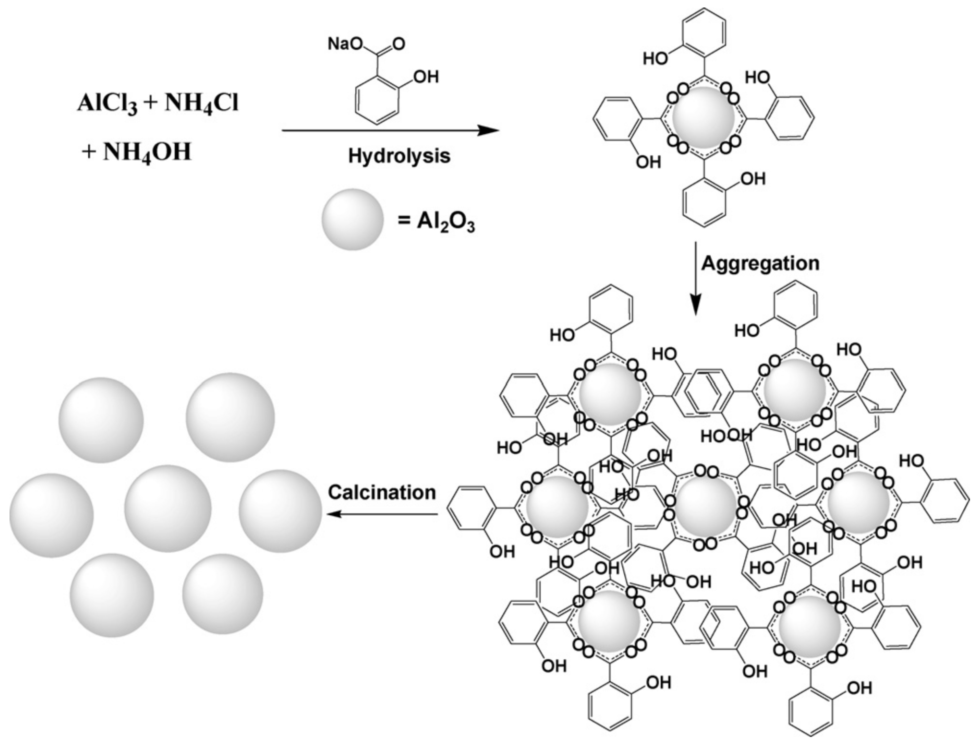

Fig. 3. Proposed templating pathway for the synthesis of mesoporous Al_2O_3.

growth of spherical nanoparticles. Further condensation and crystallization during calcination is supported by the fact that sample MA-3, which is amorphous before calcination, transforms into crystalline γ-Al_2O_3 phase (Fig. 2B(c) vis-à-vis Fig. 2A(c)) on calcination. This could cause the increase in particle size and thus consequent enhancement in the *d* spacings.

TEM image of a representative self-assembled mesoporous Al_2O_3 nanomaterial is shown in Fig. 4A (MA-2C, calcined at 773 K). As seen from the image that pores of dimension *ca.* 3–6 nm (white spots) observed throughout the image for this sample. Further, each individual nanoparticle (of dimension 30–70 nm) is seen to be consisting of self-assembly of very tiny nanocrystals. Fig. 4B represented the respective high resolution TEM image. Lattice fringes corresponding to the crystalline γ-Al_2O_3 phase is quite clear. The selected area electron diffraction (SAED) pattern of this sample is shown in Fig. 4C. These results suggested the formation of self-assembled mesoporous Al_2O_3 nanospheres with well-defined lattice planes. The diffraction spots are indexed corresponding to the γ-Al_2O_3 structure [7]. In Fig. 5 FE SEM images of these samples are shown. The samples are composed of very tiny spherical nanoparticles of 2–10 nm for different samples. Uniform and homogeneous particle size distributions are observed for all the samples. As seen from the images that for samples MA-1 and MA-2 crystal edges are sharper than that for MA-3. This could be attributed to comparatively higher synthesis temperatures for MA-3, suggesting that at high temperature the crystallization is favored.

N_2 adsorption/desorption isotherms of samples MA-1C and MA-2C are shown in Fig. 6. These isotherms could be classified as type IV isotherm characteristic of the mesoporous materials [28–33]. In these isotherms, for the relative pressure P/P_0 in between 0.01 and 0.60, the adsorption amount gradually increases for all the samples. However, after $P/P_0 > 0.6$ the N_2 uptake get saturated. The BET surface areas for the calcined samples MA-1C, MA-2C and MA-3C were 497, 403 and 231 $m^2\,g^{-1}$, respectively. Their respective pore volumes were 0.36, 34 and 0.23 $cm^3\,g^{-1}$. Pore size distributions of these samples employing BJH model (N_2 adsorption on silica as reference) suggested that MA-1C synthesized at 393 K has an average pore width of *ca.* 3.6 nm vis-à-vis *ca.* 3.4 nm for sample MA-2C synthesized at 353 K. Pore widths obtained from this N_2 sorption analysis agree well with those values obtained from TEM image analyses independently.

UV–visible spectroscopy is one of the most important analytical tools for characterizing the optical properties of the semiconductor nanocrystals. UV–visible diffuse reflectance spectrum of as-synthesized and calcined mesoporous γ-Al_2O_3 samples are shown in Fig. 7. The as-synthesized γ-Al_2O_3 material showed absorption maxima at *ca.* 253 nm and long absorption tail at *ca* 337 nm, suggesting the chemical binding of the salicylate molecules at the γ-Al_2O_3 surfaces. For the mesoporous γ-Al_2O_3 materials MA-1, MA-2 and MA-3 after template removal this band is considerably blue shifted. UV–visible diffuse reflectance spectra of calcined MA-1C sample shows absorption band at 247 nm, which corresponds to the band gap energy of 3.43 eV (shown in the inset of Fig. 7). This band gap energy is much lower than direct band gap of 6.31 eV for bulk γ-Al_2O_3 [34]. The respective as-synthesized composite material showed band gap energy of 3.24 eV. Low band gap of the composite material suggested the possible binding of the salicylate molecule at the γ-Al_2O_3 surfaces.

The thermal stability of the template-free mesoporous alumina material was estimated quantitatively from the TG-DTA profiles under air flow. When the as-synthesized sample was heated in air, three distinct weight losses were observed (Fig. 8). Initial weight loss could be attributed to the removal of physically adsorbed water molecules below 393 K. The gradual decrease in the weight in the temperature range 400–950 K involved two steps, which could be attributed to dehydration of aluminum hydroxide, and burning and subsequent removal of organic salicylate molecules present in the mesoporous Al_2O_3 material. In the temperature range 730–830 K a strong exothermic peak is observed in the DTA curve. This could be attributed to further condensation and dehydration to form crystalline mesoporous aluminum oxide nanoparticles. Further crystallization could also take place above the temperature 950 K.

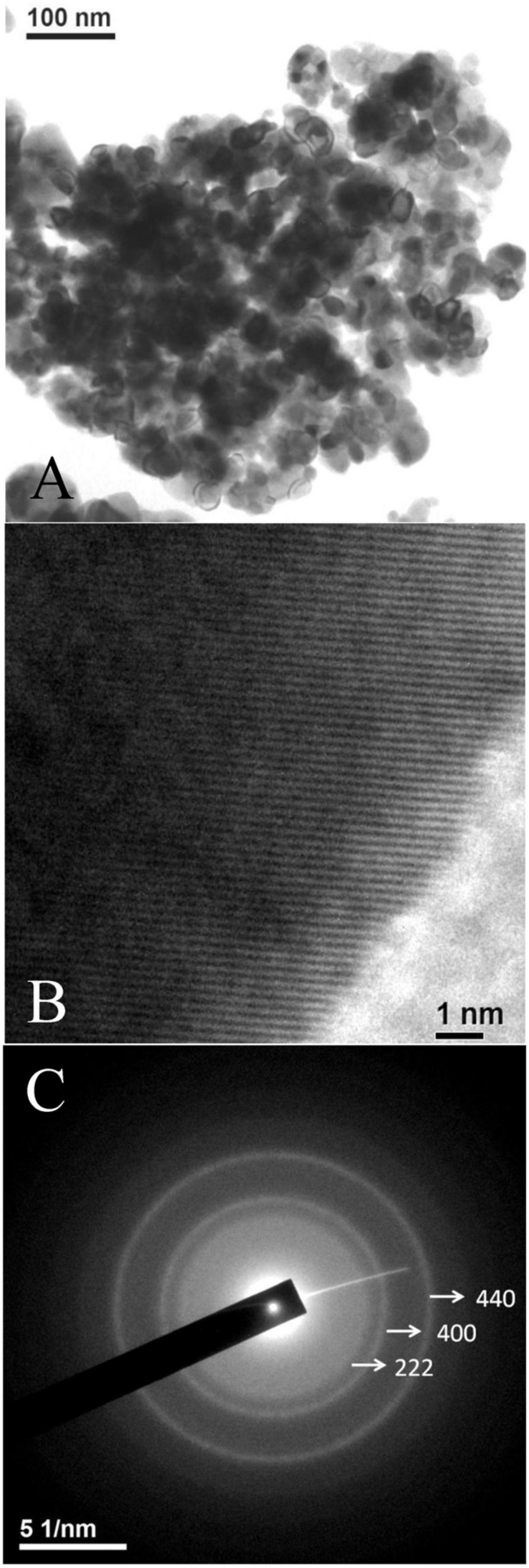

Fig. 4. TEM image of (A) self-assembled γ-Al_2O_3 nanoparticles (A), respective HRTEM image (B) and selected area electron diffraction (SAED) pattern (C) of calcined mesoporous γ-Al_2O_3 sample MA-2C.

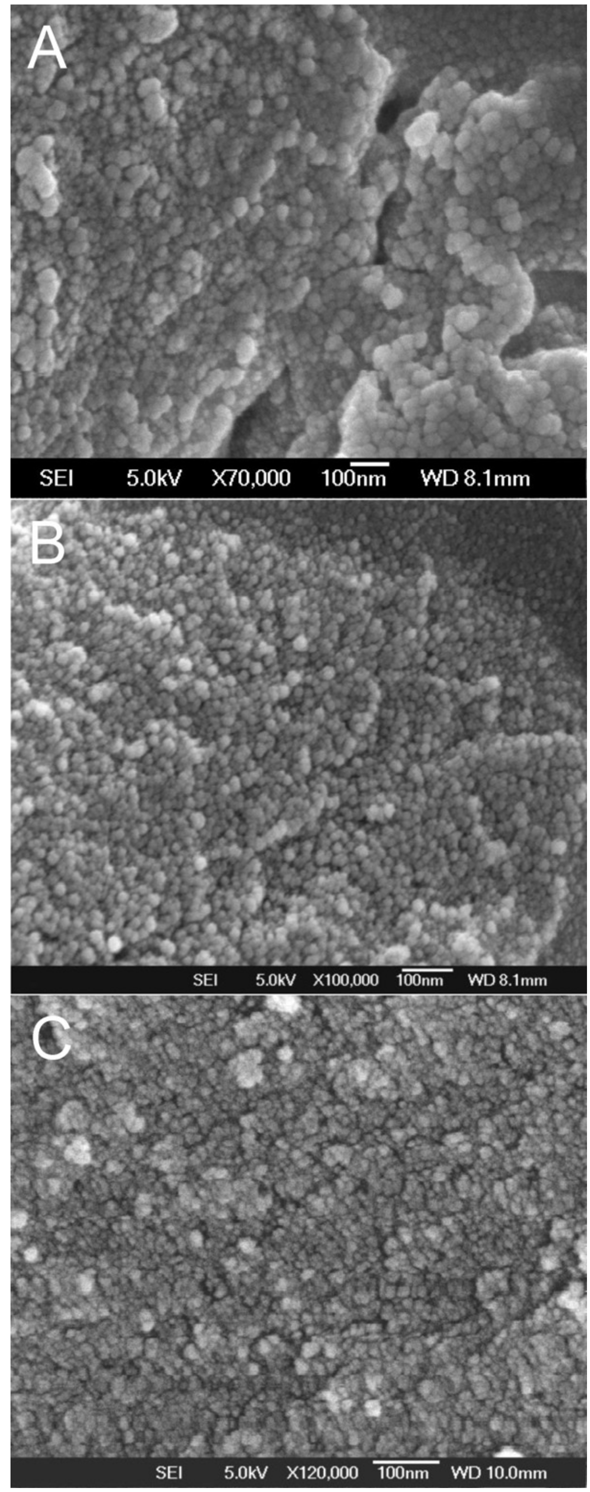

Fig. 5. FE-SEM images of mesoporous MA-1C (a), MA-2C (b) and MA-3C (c).

3.2. Adsorption studies: arsenic removal over mesoporous γ-Al_2O_3

The arsenic contents in different aqueous solutions before and after adsorption studies are shown in Table 1. As seen from Table 1 that the adsorption efficiency for MA-1C varies from *ca.* 64–86% for different stock solutions and ground water samples, whereas that for MA-2C it was *ca.* 58–81%. Commercial Al_2O_3 showed much lower adsorption efficiency for dissolved arsenic under

Table 2
Compositions of deep tube-well waters.

Sample name	Na^+ (mg/L)	K^+ (mg/L)	Ca^{2+} (mg/L)	$Fe^{2+/3+}$ (mg/L)	AsO_2^- (mg/L)
Sample 1[a]	105.20	3.21	65.96	3.75	2.57
Sample 2[b]	311.24	8.10	115.46	1.20	0.504
Sample 3[c]	35.15	2.25	43.87	7.06	0.272

[a] Ground water sample collected from the deep tube-wells located in South 24 Parganas.
[b] Ground water sample collected from the deep tube-wells located in Jadavpur.
[c] Ground water sample collected from the deep tube-wells located in Hooghly, West Bengal, India.

similar reaction conditions. Our mesoporous γ-Al_2O_3 materials also showed much larger distribution coefficients (*ca.* 3.0–6.3 × 10^3) for the removal of arsenic for all these adsorption experiments vis-à-vis commercial alumina. These values are comparable with functionalized mesoporous materials having anion exchange sites in the frameworks [30,32,35]. The results of the recycling experiment for the adsorption of dissolved arsenic are shown in Fig. 9. From this bar diagram it is clear that mesoporous γ-Al_2O_3 material can be used for repeated adsorption studies without much loss in adsorption efficiency. The composition of these tube-well waters was given in Table 2. Apart from arsenic, Na, K, Ca and Fe are the major contaminant cations present in all these water samples.

Fig. 10 shows the adsorption kinetics for arsenic(III) and arsenic(V) containing solutions studied at room temperature. Experimental results suggested that initially mesoporous γ-Al_2O_3 materials absorb arsenic oxyanions to a large extent. The high uptake of arsenic in first 2 h could be attributed to the monolayer adsorption on the mesoporous surface of MA-1C. This is followed by

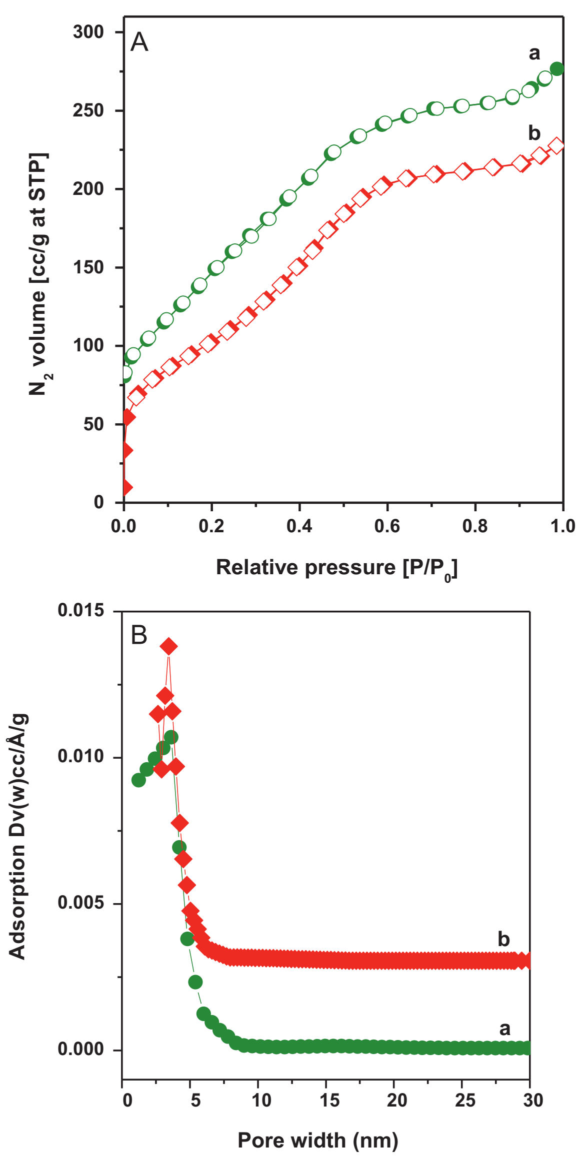

Fig. 6. (A) N_2 adsorption (●)–desorption (○) isotherms of the calcined MA-1C (a) and MA-2C (b) at 77 K. *Y* axis of plot a has been enhanced by 30 for clarity. (B) Respective pore size distributions using BJH model.

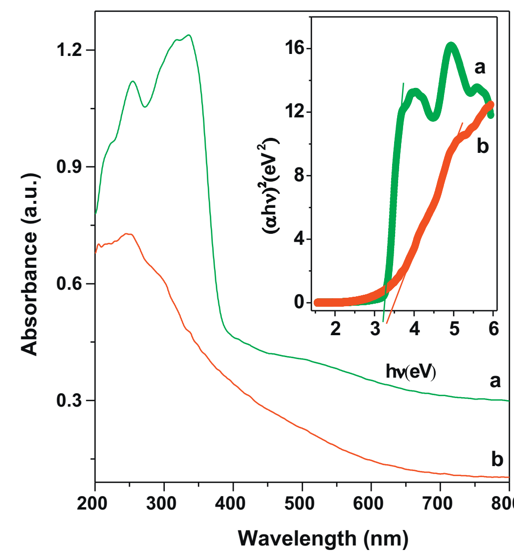

Fig. 7. UV–visible diffuse reflectance spectra of as-synthesized (a) and calcined mesoporous MA-1 (b).

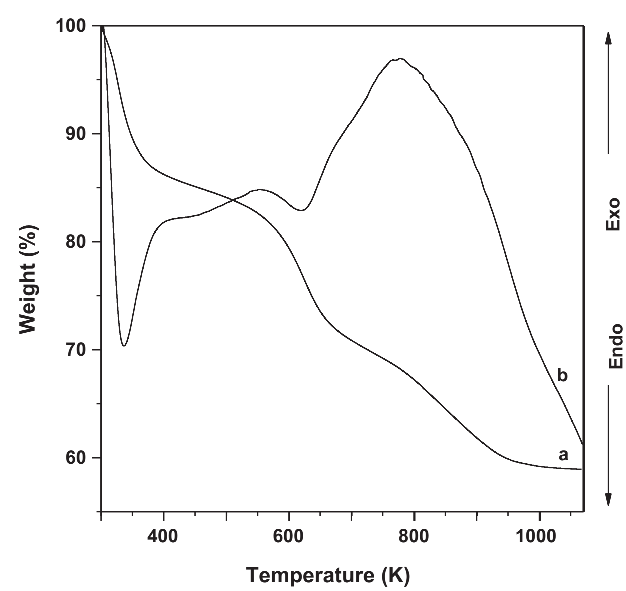

Fig. 8. TG (a) and DTA (b) curves for as-synthesized sample MA-1.

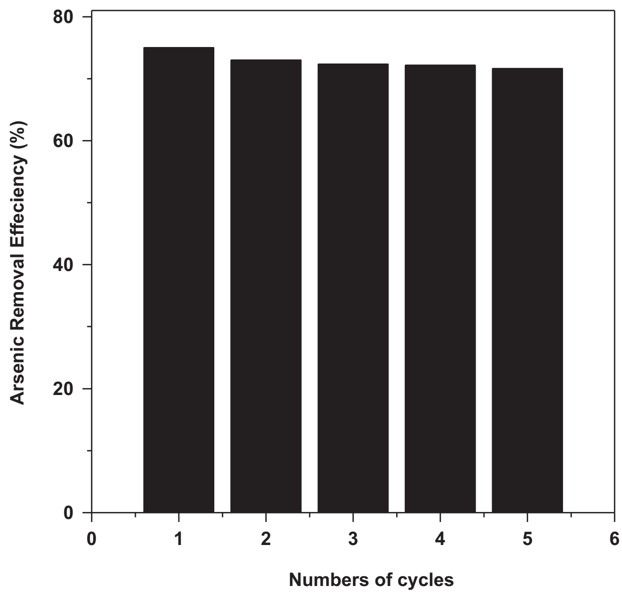

Fig. 9. Arsenic removal efficiency cycles over mesoporous alumina MA-1C sample.

multilayer adsorption on prolonged reaction times. So the adsorption amount gradually increased with time. It is interesting to note that throughout these adsorption studies adsorption amounts for AsO_4^{3-} remained higher than that of AsO_2^-, suggesting larger affinity for As(V) over As(III) at the mesoporous alumina surface.

The pH dependent adsorption experiments (envelope) were carried out at AsO_2^- concentration of 100 ppb at room temperature for 6 h under vigorous stirring with MA-1C. The results are shown in Fig. 11. The pH of the solutions was controlled by using commercially available buffer solutions. The material showed highest efficiency for the removal of arsenic at *ca.* pH = 6.0 and with increasing or decreasing the pH, adsorption efficiency has been decreased. This could be due to the fact that at high pH value the Lewis acid sites of materials are blocked by hydroxide anion, whereas at low pH values some oxyanions are present in the form of undissociated H_3AsO_4/H_3AsO_3. Thus our experimental observations

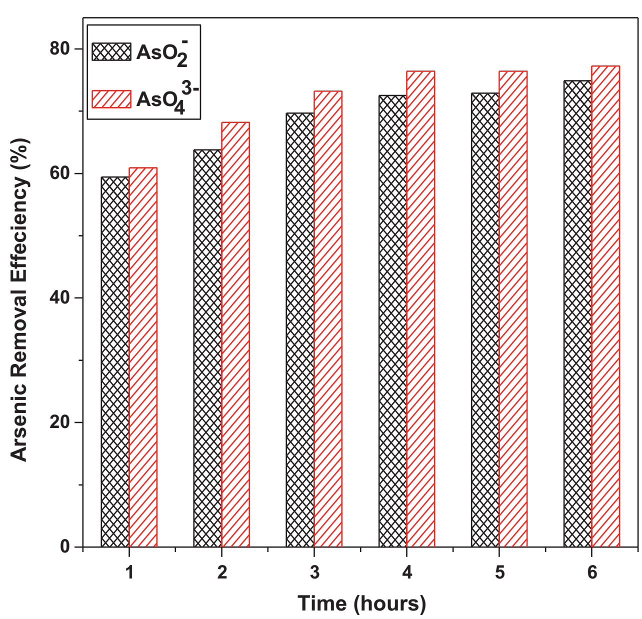

Fig. 10. The arsenic adsorption kinetics of both As(III) and As(V) as function of time over MA-1C material.

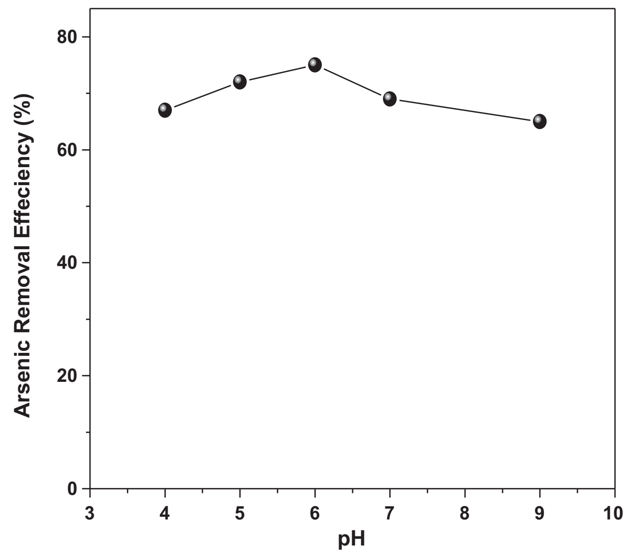

Fig. 11. Arsenic removal efficiency of MA-1C material as a function of pH.

suggested that the arsenic removal efficiency over mesoporous γ-Al_2O_3 material remained stable after repeated adsorption studies and at different pHs. Hence, these self-assembled tiny spherical nanoparticles of mesoporous γ-Al_2O_3 have huge potential to be utilized as adsorbent for the removal of arsenic from polluted water.

4. Conclusions

From the above experimental results we can conclude that self-assembled mesoporous γ-Al_2O_3 spherical nanoparticles can be synthesized hydrothermally by using the supramolecular-assembly of sodium salicylate as a template. Salicylate anions ligated with the positively charged Al(III) centers through covalent interaction during the synthesis process. Further, the H-bonding interactions between the phenolic –OH groups could help to form the supramolecular structure of salicylate moieties during synthesis, which on calcination generate mesopores of dimension 3–6 nm depending upon the synthesis temperatures. The synthesis strategy described herein for high surface area mesoporous γ-Al_2O_3 spherical nanoparticles and its excellent adsorption capacity for dissolved arsenic from the respective aqueous solution may contribute significantly in developing an efficient adsorption media for the treatment of arsenic-contaminated water.

Acknowledgements

AKP and AD thank CSIR, New Delhi for their respective senior research fellowships. AB wishes to thank DST New Delhi for providing instrumental facility through Nano Mission Initiative.

References

[1] Y. Yin, A.P. Alivisatos, Colloidal nanocrystal synthesis and the organic–inorganic interface, Nature 437 (2005) 664–670.
[2] B.L. Cushing, V.L. Kolesnichenko, C.J. O'Connor, Recent advances in the liquid-phase syntheses of inorganic nanoparticles, Chem. Rev. 104 (2004) 3893–3946.
[3] S.G. Kwon, T. Hyeon, Colloidal chemical synthesis and formation kinetics of uniformly sized nanocrystals of metals, oxides, and chalcogenides, Acc. Chem. Res. 41 (2008) 1696–1709.
[4] N.R. Jana, Y.F. Chen, X.G. Peng, Size- and shape-controlled magnetic (Cr, Mn, Fe, Co, Ni) oxide nanocrystals via a simple and general approach, Chem. Mater. 16 (2004) 3931–3935.
[5] K.J. Rao, K. Mahesh, S. Kumar, A strategic approach for preparation of oxide nanomaterials, Bull. Mater. Sci. 28 (2005) 19–24.
[6] M. Niederberger, Nonaqueous sol–gel routes to metal oxide nanoparticles, Acc. Chem. Res. 40 (2007) 793–800.

[7] J. Cejka, Organized mesoporous alumina: synthesis, structure and potential in catalysis, Appl. Catal. A: Gen. 254 (2003) 327–338.
[8] M. Trueba, S.P. Trasatti, γ-Alumina as a support for catalysts: a review of fundamental aspects, Eur. J. Inorg. Chem. 17 (2005) 3393–3403.
[9] M.H. Yuan, C.Y. Chang, J.L. Shie, C.C. Chang, J.H. Chen, W.T. Tsai, Destruction of naphthalene via ozone-catalytic oxidation process over Pt/Al_2O_3 catalyst, J. Hazard. Mater. 175 (2010) 809–815.
[10] K. Shimizu, M. Nishimura, A. Satsuma, γ-Alumina-supported silver cluster for N-benzylation of anilines with alcohols, ChemCatChem 1 (2009) 497–503.
[11] M. Paul, N. Pal, A. Bhaumik, Mesoporous nickel–aluminum mixed oxide: a promising catalyst in hydride-transfer reactions, Eur. J. Inorg. Chem. 32 (2010) 5129–5134.
[12] X.-S. Fang, C.-H. Ye, X.-X. Xu, T. Xie, Y.-C. Wu, L.-D. Zhang, Synthesis and photoluminescence of α-Al_2O_3 nanowires, J. Phys.: Condens. Matter 16 (2004) 4157–4163.
[13] J. Robertson, B. Falabretti, Band offsets of high K gate oxides on III–V semiconductors, J. Appl. Phys. 100 (2006) 014111.
[14] G. Lee, C. Chen, S.-T. Yang, W.-S. Ahn, Enhanced adsorptive removal of fluoride using mesoporous alumina, Microporous Mesoporous Mater. 127 (2010) 152–156.
[15] X.Y. Zhang, J. Zhao, A.V. Whitney, J.W. Elam, R.P. Van Duyne, Ultrastable substrates for surface-enhanced Raman spectroscopy: Al_2O_3 overlayers fabricated by atomic layer deposition yield improved anthrax biomarker detection, J. Am. Chem. Soc. 128 (2006) 10304–10309.
[16] D. Mohana, C.U. Pittman Jr., Arsenic removal from water/wastewater using adsorbents – a critical review, J. Hazard. Mater. 142 (2007) 1–53.
[17] M. Jose Medrano, R. Boix, R. Pastor-Barriuso, M. Palau, J. Damian, R. Ramis, J.L. del Barrio, A. Navas-Acien, Arsenic in public water supplies and cardiovascular mortality in Spain, Environ. Res. 110 (2010) 448–454.
[18] J.F. Martinez-Villafane, C. Montero-Ocampo, A.M. Garcia-Lara, Energy and electrode consumption analysis of electrocoagulation for the removal of arsenic from underground water, J. Hazard. Mater. 172 (2009) 1617–1622.
[19] A. Bhaumik, S. Samanta, N.K. Mal, Efficient removal of arsenic from polluted ground water using LDH exchanger, Indian J. Chem. A 44 (2005) 1406–1409.
[20] Y. Jeong, M. Fan, S. Singh, C.L. Chuang, B. Saha, H. van Leeuwen, Evaluation of iron oxide and aluminum oxide as potential arsenic(V) adsorbents, Chem. Eng. Process. 46 (2007) 1030–1039.
[21] K. Hristovski, A. Baumgardner, P. Westerhoff, Selecting metal oxide nanomaterials for arsenic removal in fixed bed columns: from nanopowders to aggregated nanoparticle media, J. Hazard. Mater. 147 (2007) 265–274.
[22] W.L. Hu, F. Zheng, B. Hu, Simultaneous separation and speciation of inorganic As(III)/As(V) and Cr(III)/Cr(VI) in natural waters utilizing capillary microextraction on ordered mesoporous Al_2O_3 prior to their on-line determination by ICP-MS, J. Hazard. Mater. 151 (2008) 58–64.
[23] H. Park, H. Choi, As(III) removal by hybrid reactive membrane process combined with ozonation, Water Res. 45 (2011) 1933–1940.
[24] G.K. Prasad, P.V.R.K. Ramacharyulu, B. Singh, A.R. Srivastava, K. Ganesan, R. Vijayaraghavan, Decontamination of Yperite using mesoporous mixed metal oxide nanocrystals, J. Hazard. Mater. 183 (2010) 847–852.
[25] Z.R. Zhang, T.J. Pinnavaia, Mesostructured gamma-Al_2O_3 with a lathlike framework morphology, J. Am. Chem. Soc. 124 (2002) 12294–12301.
[26] Q. Yuan, A.-X. Yin, C. Luo, L.-D. Sun, Y.-W. Zhang, W.-T. Duan, H.-C. Liu, C.-H. Yan, Facile synthesis for ordered mesoporous γ-aluminas with high thermal stability, J. Am. Chem. Soc. 130 (2008) 3465–3472.
[27] A.K. Patra, S.K. Das, A. Bhaumik, Self-assembled mesoporous TiO_2 spherical nanoparticles by a new templating pathway and its enhanced photoconductivity in the presence of an organic dye, J. Mater. Chem. 21 (2011) 3925–3930.
[28] H. Li, L. Zhang, H.X. Dai, H. He, Facile Synthesis and unique physicochemical properties of three-dimensionally ordered macroporous magnesium oxide, gamma-alumina, and ceria–zirconia solid solutions with crystalline mesoporous walls, Inorg. Chem. 48 (2009) 4421–4434.
[29] R.E. Williford, G.E. Fryxell, X.S. Li, R.S. Addleman, Mechanism of hierarchical porosity formation in silica thin films using cellulose nitrate, Microporous Mesoporous Mater. 84 (2005) 201–210.
[30] D. Chandra, A. Bhaumik, N.K. Mal, Novel mesoporous silicotinphosphate molecular sieve with high anion exchange capacity, J. Mol. Catal. A: Chem. 247 (2006) 216–221.
[31] P. Delaney, C. McManamon, J.P. Hanrahan, M.P. Copley, J.D. Holmes, M.A. Morris, Development of chemically engineered porous metal oxides for phosphate removal, J. Hazard. Mater. 185 (2011) 382–391.
[32] D. Chandra, B.K. Jena, C.R. Raj, A. Bhaumik, Functionalized mesoporous cross-linked polymer as an efficient host for loading gold nanoparticles and its electrocatalytic behavior for reduction of H_2O_2, Chem. Mater. 19 (2007) 6290–6296.
[33] D. Chandra, A. Bhaumik, New functionalized mesoporous polymer having high efficiency for the removal of pollutant anions, J. Mater. Chem. 19 (2009) 1901–1907.
[34] W.Y. Ching, Y.N. Xu, First-principles calculation of electronic, optical, and structural properties of alpha-Al_2O_3, J. Am. Ceram. Soc. 77 (1994) 404–411.
[35] K. Murakami, X. Yu, S. Watanabe, T. Kato, Y. Inoue, K. Sugawara, Synthesis of thermosensitive polymer/mesoporous silica composite and its temperature dependence of anion exchange property, J. Colloid Interface Sci. 354 (2011) 771–776.